THE JOURNAL OF PHYSICAL CHEMISTRY C

Article

pubs.acs.org/JPCC

Unexpected Behavior of Copper in Modified Ferrites during High Temperature WGS Reaction—Aspects of $Fe^{3+} \leftrightarrow Fe^{2+}$ Redox Chemistry from Mössbauer and XPS Studies

Gunugunuri K. Reddy,[†] P. Boolchand,[‡] and Panagiotis G. Smirniotis*,[†]

[†]Chemical Engneering Program, School of Energy, Environmental, Biological and Medicinal Engineering, University of Cincinnati, Cincinnati, Ohio 45221, Unites States

[‡]Department of Electrical and Computer Science Engineering, University of Cincinnati, Cincinnati, Ohio 45221, United States

ABSTRACT: We report dynamic alternation of the redox chemistry of the Fe^{3+}/ Fe^{2+} couple in magnetite during high temperature water−gas shift reaction in Cu codoped M-modified ferrite catalysts. Various hematitic solid solutions of the type Fe_2O_3−M_xO_y−CuO_x with M = Cr, Ce, Ni, Co, Mn, and Zn are synthesized using the industrially economical and environmentally friendly coprecipitation method. Interestingly, Cu shows an unusual effect in the M-modified ferrites during the high temperature WGS reaction. Remarkably, our shift activity measurements reveal that Cu act as a promoter for all M-modified ferrites with M = Cr, Ni, Co, Mn, and Zn except M = Ce. For the latter case, Cu acts as an inhibitor for the high temperature WGS reaction. Temperature programmed reduction measurements (TPR) show that Cu selectively promotes the reduction of hematite (Fe_2O_3) to magnetite (Fe_3O_4) in all modified ferrite catalysts. However, Cu does not promote the reduction of magnetite to wustite or reduction of other metal oxide present in the ferrite expect for M = Ce. Mössbauer effect studies show distortions in the Fe local environments when Cu is codoped in magnetite. These distortions are reflected in the internal magnetic field at octahedral (O_h) sites with characteristic isomer shift "δ". The Mössbauer spectra and XPS measurements show that Cu plays a different role on Fe^{3+}/Fe^{2+} redox chemistry in the bulk and surface. During the activation, some of the Cu enters at the O_h sites of the magnetite and replaces Fe^{2+} ions and the remaining Cu forms metallic Cu species except for the Fe/Ce. This dual promotional role is responsible for the observed high temperature WGS activity in Cu codoped M-modified ferrites. For M = Ce, characterization studies show that both Ce and Cu enter the iron oxide lattice substitutionally upon activation and form the wustite (FeO) phase along with the magnetite phase. The formation of wustite (FeO) is responsible for the decreased WGS activity upon Cu codoping of Fe/Ce catalyst.

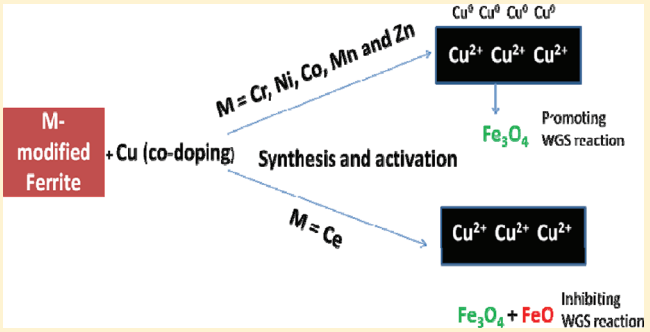

1. INTRODUCTION

Spinel ferrites have been studied for many years to elucidate their catalytic behavior and their correlated nature to structural properties especially to understand the catalytic reactions.[1−3] The spinels AB_2O_4 constitute one of the most interesting families of crystalline compounds. The dynamic alternation between stoichiometry and nonstoichiometry in spinel ferrites (AB_2O_4) is an important feature that is exploited in gas reactions.[4] The A and B cations can occupy two different sites in the spinel structure, e.g., octahedral (O_h) and tetrahedral (T_d) sites within the FCC oxygen sublattice. Substitution of "Fe" sites in an AB_2O_4 type of ferrite with other cations leads to the crystallization of either an inverse or a mixed spinel with the structural composition $A_{1-\delta}B_{\delta}[A_{\delta}B_{2-\delta}]O_4$, where δ provides the degree of inversion.[5] The cation distributions in spinels are of considerable interest for a better understanding of the correlation between structures and physical and chemical properties such as magnetism, conductivity, and catalytic activity, which are dependent on the nature of ions, their charge states, and their occupancy at O_h and T_d sites. Metal doping at Fe sites is expected to strongly modify the redox properties of the resultant ferrites.[6]

Recently, water−gas shift (WGS) reaction using membrane reactors has become attractive largely because hydrogen can be selectively permeate through a membrane, making complete conversion possible.[7] It is very difficult to develop catalysts for these membranes, since they operate at high temperatures (450−550 °C) and high pressures (5−20 bar).[8−11] Magnetite (Fe_3O_4) spinels are active catalysts for the conventional high-temperature WGS reaction.[12−14] In magnetite-type (Fe_3O_4) crystalline structures, O_h sites are occupied by Fe^{2+} and Fe^{3+}, while T_d sites are occupied by Fe^{3+} ions only. Reithwisch and Dumesic studied a number of spinel ferrite structures (normal, mixed, and inverse) and concluded that only inverse or mixed magnetite spinels are active catalysts for WGS reaction.[15] The rapid electron exchange between Fe^{3+} and Fe^{2+} ions present at

Received: February 2, 2012
Revised: May 1, 2012
Published: May 1, 2012

O_h sites is largely responsible for the high WGS activity. The significant role of $Fe^{2+} \Leftrightarrow Fe^{3+}$ redox exchange in the WGS reaction was also demonstrated by Boreskov.[16] The catalytic activity of magnetite depends on the stabilization and covalency of the $Fe^{2+} \Leftrightarrow Fe^{3+}$ redox couple, which in turn depends on the nature of ions, their oxidation states, and the relative O_h and T_d occupancy in the magnetite spinel host. If one can facilitate T_d sites to expand and O_h sites to contract, an improvement in covalency of the system results and promotes electron hopping between these sites ($Fe^{2+} \Leftrightarrow Fe^{3+}$), resulting in improved WGS activity.[17,18] It is well-known that Cu is a very good promoter for the high-temperature WGS reaction, although its promotional function is still debated. The physical and chemical state of Cu species on surface and in the bulk plays an important role in the WGS reaction. We know that the incorporation of Cu in iron oxide modifies the acid−base and redox properties of the spinel lattice.[19,20] Idakiev et al.[21] reported that Cu^{2+} cations form a solid solution with Fe^{2+} and Fe^{3+} and modify electronic properties of the Fe_3O_4 structure during WGS reduction−oxidation sequences. According to crystal field theory, we might expect Cu^{2+}, with a d^9 electron configuration and $\Delta = 0.6$, preferentially takes on octahedral co-ordination.[22] However, the situation is complicated by the fact that Cu^{2+} undergoes Jahn−Teller distortions at both O_h and T_d coordinated environments. In the magnetite, the precise location of Cu^{2+} ions in solid solution is still unclear. Hence, it is quite important to investigate in more detail the distribution of Cu ions in the magnetite spinels and their role in promoting effect in the WGS reaction.

In our previous study, we examined metal doped magnetite spinels (Fe:M) with the following metals: M = Cr, Mn, Co, Ni, Cu, Zn, and Ce and their catalytic activity in the high temperature WGS reaction.[23] The present study is aimed at investigating the role of Cu codoping on the structure and aspects of $Fe^{3+} \leftrightarrow Fe^{2+}$ redox chemistry in these M-modified spinels. For this purpose, a series of Cu codoped modified ferrites of type Fe:M:Cu (M = Cr, Ce, Ni, Co, Mn, and Zn) with atomic ratios 10:1:0.25 were synthesized by the industrially economical and environmentally friendly coprecipitation method. The high temperature WGS reaction was performed at temperatures of 450 and 550 °C and a steam to CO ratio of 3.5. Interestingly, the Cu codoping in M-modified spinels results in different behavior for the Fe/Ce compared to the remaining spinels. In all cases, Cu acts as a promoter except in the case of Fe/Ce. In the latter case, Cu acts as an inhibitor. Temperature-programmed reduction measurements show that Cu codoping selectively promotes the hematite to magnetite transformation in all the M-modified spinels. On the other hand, Cu promotes hematite to magnetite, magnetite to wustite, and surface ceria reduction temperatures in the Fe/Ce spinel. Structural characterization measurements show that Cu ions selectively substitute the O_h sites in magnetite to form solid solutions. Surface characterization measurements suggest that Cu provides active surface assemblies for the WGS reaction. These two features of the structure, in tandem, are thought to promote catalytic performance over a wide temperature range.

2. EXPERIMENTAL SECTION

2.1. Catalyst Preparation. The ammonia assisted coprecipitation route is explored for high-yield preparation of various M-modified and Cu codoped modified ferrite spinels at atomic ratios of 10:1:0.25. In a typical preparation, calculated amounts of iron nitrate, copper nitrate, and the corresponding dopant metal nitrate were dissolved separately in deionized water and mixed together. Dilute aqueous ammonia was added gradually dropwise to the aforementioned mixture solutions, with vigorous stirring, until precipitation was complete (pH ≈ 9). The supernatant liquid was analyzed for nitrate ions by adding about 1 mL of concentrated sulfuric acid to 10 mL of the supernatant, while the formation of $[Fe(NO)]^{2+}$ can be detected by a brown ring.[24] The formation of a brown ring was not observed in all the cases. Thus, the obtained precipitate gels were further aged overnight, and filtered off. The obtained cakes were oven-dried at 80 °C for 12 h and finally calcined at 500 °C for 3 h in an inert environment. The rate of heating as well as cooling was always maintained at 5 °C min^{-1}.

2.2. Catalyst Characterization. *2.2.1. Surface Area and Pore Size Distribution Analysis.* The BET surface areas were obtained by N_2 adsorption on a Micromeritics 2010 Instrument. Prior to the analysis, samples were oven-dried at 120 °C for 12 h and flushed with argon for 3 h. All samples were degassed at 300 °C under a vacuum before analysis.

2.2.2. X-ray Diffraction Measurements. Powder X-ray diffraction (XRD) patterns were recorded on a Phillips Xpert diffractometer using a nickel-filtered Cu Kα (0.154056 nm) radiation source. The intensity data were collected over a 2θ range of 3−80° with a 0.02° step size and using a counting time of 1 s per point. Crystalline phases were identified by comparison with the reference data from ICDD files. The average crystallite size was estimated with the help of the Debye−Scherrer equation, using the XRD data of all prominent lines.[25] Lattice parameter estimations were carried out by employing standard indexation methods using the intensity of high 2θ peaks (311).[25−27]

2.2.3. TPR Measurements. The temperature-programmed reduction (TPR) with hydrogen of various catalyst samples was performed by means of an automated catalyst characterization system (Micromeritics, model AutoChem II 2920), which incorporates a thermal conductivity detector (TCD). The experiments were carried out at a heating rate of 5 °C/min. The reactive gas composition was H_2 (10 vol %) in argon. The flow rate was fixed at 10 mL/min (STP). The total reactive gas consumption during TPR analysis was measured. The TPR measurements were carried out following activation after cooling the sample in helium flow to 50 °C. The sample was then held at 50 °C under flowing helium to remove the remaining adsorbed oxygen until the TCD signal returned to the baseline. Subsequently, the TPR experiments were performed up to a temperature of 800 °C. The water formed during the reduction was removed by using a trapper. The gas stream coming from the reactor was passed through a trapper before the gas entered into the GC. A mixture of iso-propanol and liquid nitrogen was used in the trapper to trap the formed water during the TPR experiment.

2.2.4. Mössbauer Spectral Analysis. ^{57}Fe Mössbauer spectra were recorded in a transmission geometry using a constant acceleration spectrometer with a liquid helium metal dewar.[28] Experiments were performed both at room temperature and at liquid nitrogen temperature. A 20 mCi portion of ^{57}Co (Rh) was used as an emitter, and the spectrometer was calibrated using a α-Fe foil, and using isomer shift of Rh wrt α-Fe at −0.15 mm s^{-1}. Line widths, on the inner two lines of α-Fe were typically found to be 0.22 mm/s. An 80 mg quantity of the oxide catalyst as a fine powder was spread on a thin Teflon sheet using GE varnish as a binder, and used as an absorber. A

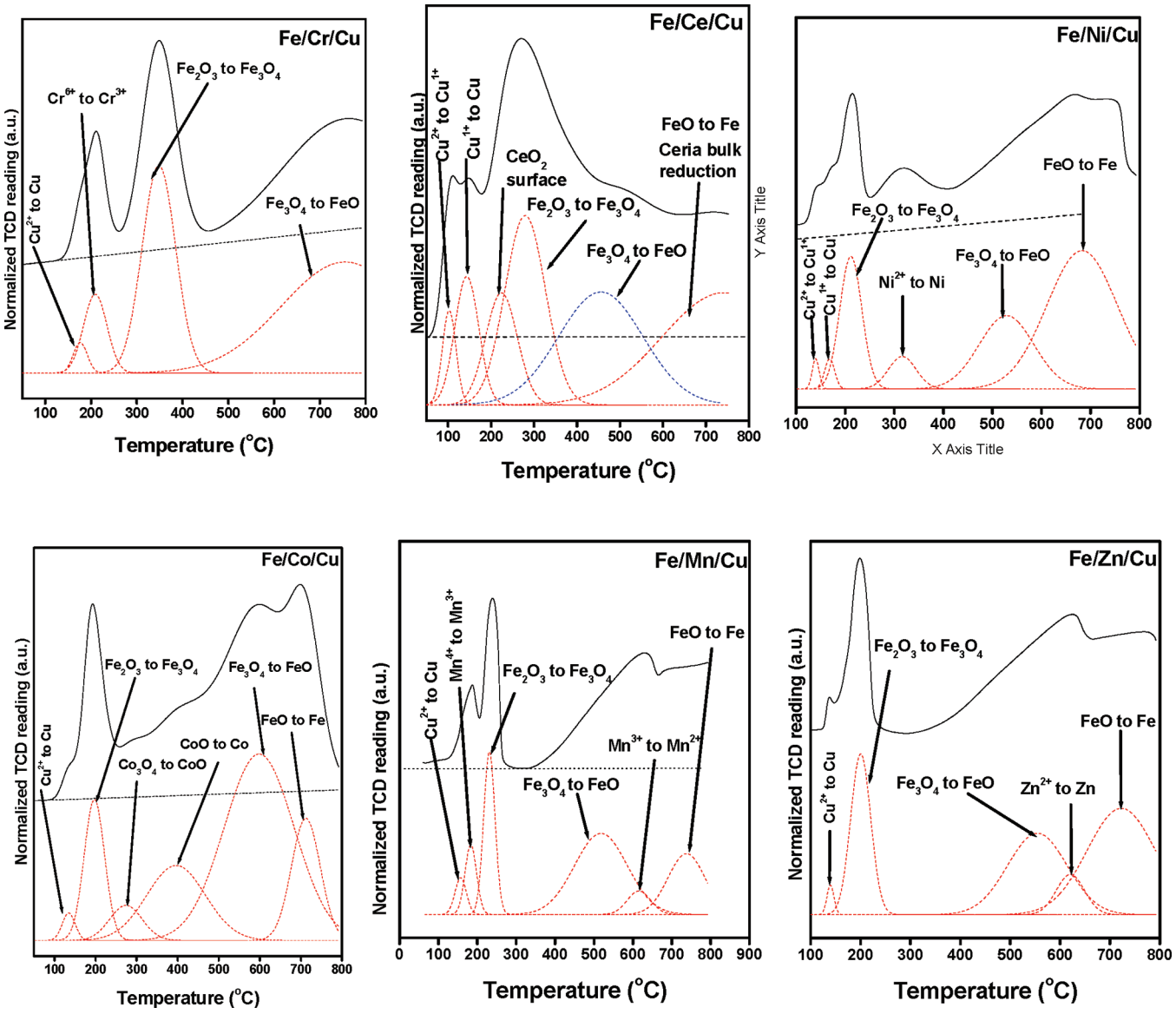

Figure 1. TPR profiles of copper codoped M-modified ferrite catalysts.

typical run lasted 48 h and baseline counts per channel of two millions.

2.2.5. XPS Measurements. The X-ray photoelectron spectroscopy (XPS) measurements were performed on a Pyris VG Thermo Scientific spectrometer using Al Kα (1486.6 eV) radiation as the excitation radiation. Charging of the catalyst samples was corrected by setting the binding energy of the adventitious carbon (C 1s) at 284.6 eV. The XPS analysis was performed at ambient temperature and at pressures typically on the order of $<10^{-8}$ Torr. Prior to analysis, the samples were outgassed under a vacuum for 4 h. The Fe 2p spectra were deconvulated to deduce the Fe^{2+}/Fe^{3+} on the surface.

2.3. Catalyst Activity. The WGS reaction was carried out in a vertical down flow fixed bed differential ceramic microreactor (i.d. 0.635 cm) at atmospheric pressure. In a typical experiment, ca. 0.1 g of powdered catalyst was placed between two plugs of quartz wool. The reactor was placed vertically inside a programmable tubular furnace (Lindberg), which was heated electrically. The catalyst pretreatment involves the partial reduction of hematite (Fe_2O_3) to magnetite (Fe_3O_4) using a process gas (mixture of H_2, CO, CO_2 (99.9% pure gases), and water vapor)[29−31] with a reductant to oxidant ratio of R = 1.4 (R = [CO] + [H_2]/[CO_2] + [H_2O]). Prior to the reaction, the catalyst was pretreated in flowing process gas at 400 °C for 4 h. It is important to avoid over-reduction of the magnetite active phase to lower carbides, oxides, or metallic iron phases. Metallic iron phases are active catalysts for methanation and Fischer−Tropsch processes.[29] The rate of heating and cooling was always maintained at 5 °C min^{-1}. The gas flows were regulated through precalibrated mass flow controllers with digital read-out unit (MKS instruments). Water was injected into the system through a motorized syringe pump (Cole-Parmer type 74900) to generate steam. The entire system was kept at 200 °C by using heating tapes. Before pretreatment, the reactor setup was flushed with an inert gas; the pretreatment gas mixture was initialized only after the catalytic system had attained temperatures higher than 150 °C. The experiments were performed at temperatures of 450 and 550 °C using a constant steam to CO ratio of 3.5. The gas hourly space velocity of 60 000 h^{-1} was maintained in all the experiments. The product stream coming from the reactor was passed through an ice cooled trap to condense water, after

dx.doi.org/10.1021/jp301090d | J. Phys. Chem. C 2012, 116, 11019−11031

which, the product gases were analyzed with an online TCD (Gow Mac series 550 thermal conductivity detector) having a porapak Q column for separation of the gases. This TCD was interfaced to a personal computer using a peak simple chromatography data system. The post analyses of the results were done on the peak simple 2.31 software. The product gas was injected through a six-port valve, and sampling was performed every 20 min intervals. In this study, the reported values of conversions correspond to steady-state values at 12 h on stream.

3. RESULTS AND DISCUSSION

Catalyst Activation. As we discussed earlier, magnetite is the active phase for the high temperature water−gas shift reaction. Before the water−gas shift reaction, the hematite phase was converted into the magnetite phase in a controlled atmosphere by prereduction. In the present study, prereduction was carried out in the presence of process gas at 400 °C for 4 h. The process gas is a mixture of CO, CO_2, H_2, and water vapor. The representative reactions are shown as follows:

$$3Fe_2O_3 + H_2 \rightarrow 2Fe_3O_4 + H_2O,$$
$$\Delta H = -16.3\ \text{kJ/mol}$$

$$3Fe_2O_3 + CO \rightarrow 2Fe_3O_4 + CO_2,$$
$$\Delta H = +24.8\ \text{kJ/mol}$$

The ratio (also called reduction factor R) of hydrogen and CO (oxidant) to water vapor and CO_2 (reductant) for the activation step determine the equilibrium of Fe^{2+} and Fe^{3+} ions in octahedral sites. With commonly used process gases, the catalyst is more reduced than necessary to reach a state of equilibrium. In this way, more Fe_3O_4 is created, which forms the stable state. If the ratio is low, then all the hematite is not converted to magnetite. If the ratio is high, over-reduction to FeO or Fe may occur. Over-reduction of the catalyst to FeO or Fe causes the loss of the active component (Fe_3O_4) as well as the physical damage of the catalyst.[32] In such a case, a damaging hot spot can form during the reaction due to exothermic methanation, for which metallic iron is known to be a good catalyst.[33] Also, metallic iron is an active component for Fischer−Tropsch reactions. Thus, it is very desirable to avoid the over-reduction of the Fe_3O_4 during prereduction. In the present study, R = 1.4 was utilized, where $R = [(CO) + (H_2)]/[(CO_2) + (H_2O)]$.

Water−Gas Shift Activity. The WGS activity results of various M-modified ferrite and Cu codoped modified ferrite catalysts are presented in Figures 2 and 3, respectively, at two temperatures. In this study, the WGS reaction was performed at a constant steam to CO ratio of 3.5. A relatively high-space velocity of 60 000 h^{-1} was maintained in all experiments. The WGS reaction was performed at temperatures of 450 and 550 °C. On the whole, the WGS operating conditions were chosen to mimic conditions found in a membrane reactor. The reported conversion values were taken once the reaction reached steady state. In general, with increasing temperature from 450 to 550 °C, the WGS activity was found to increase. No pressure drop across the catalyst bed was observed during the experiments nor was CH_4 detected in the effluent stream. Interestingly, our shift activity results reveal that Cu acts as a promoter for all the M-modified ferrite catalysts except for the Fe/Ce catalyst. It acts as an inhibitor for the Fe/Ce catalyst.

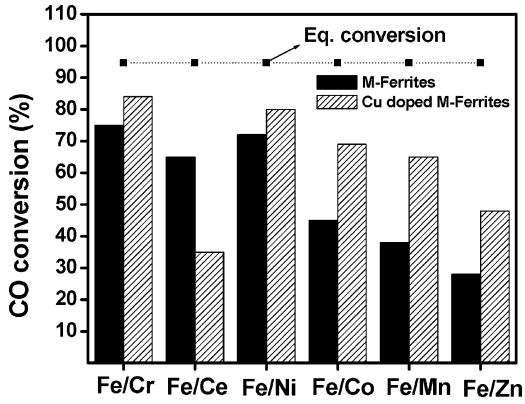

Figure 2. WGS activity results of various M-modified and copper codoped modified ferrite catalysts (temperature = 450 °C, WHSV = 60 000 h^{-1}, steam to CO ratio = 3.5).

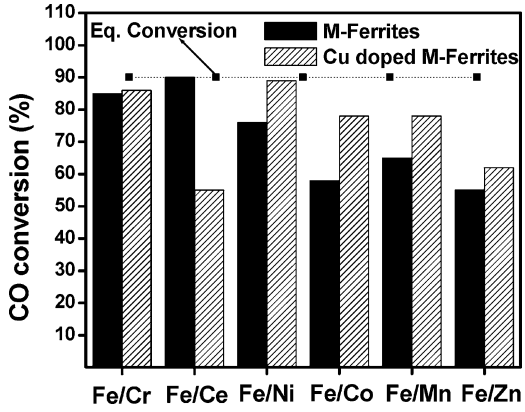

Figure 3. WGS activity results of various M-modified and copper codoped modified ferrite catalysts (temperature = 550 °C, WHSV = 60 000 h^{-1}, steam to CO ratio = 3.5).

When the reaction temperature increased from 450 to 550 °C, the activity of Fe/Ce increased from 30 to 82%. The higher activity of Fe/Ce at a higher reaction temperature is because both iron and ceria undergo a facile charge transfer reaction between $Fe^{3+} \leftrightarrow Fe^{2+}$ and $Ce^{4+} \leftrightarrow Ce^{3+}$ redox couples, respectively; the synergism between the two couples could be responsible for the improved WGS activity.[34] Additionally, at higher temperatures, the rapid oxygen exchange between the Ce^{3+}/Ce^{4+} redox couple as well as the improvement in the oxygen storage capacity of ceria[35] help the iron to keep its shift activity high. To explain the interesting behavior of Cu, we used various characterization techniques like Mössbauer, TPR, and XRD. Among the various catalysts, Fe/Ce catalyst exhibits higher CO conversions at the highest reaction temperature (550 °C) investigated. Then, the effect of H_2S content was investigated on the water−gas shift activity of Fe/Ce. Figure 4 shows the effect of H_2S content on the water−gas shift activity of Fe/Ce. No deactivation was observed up to 1000 ppm of H_2S. In general, in the presence of sulfur, the catalyst becomes sulfided with Fe_3O_4 and thus converts to FeS.[36,37] In the present study, in the presence of sulfur, no formation of FeS was observed from the XPS studies after the WGS reaction. This is probably due to the resistance of ceria to sulfurization. Ceria stabilizes magnetite from sulfiding during the WGS reaction. Moreover, at higher reaction temperatures, the adsorption and desorption phenomena of sulfur are very rapid.

dx.doi.org/10.1021/jp301090d | J. Phys. Chem. C 2012, 116, 11019−11031

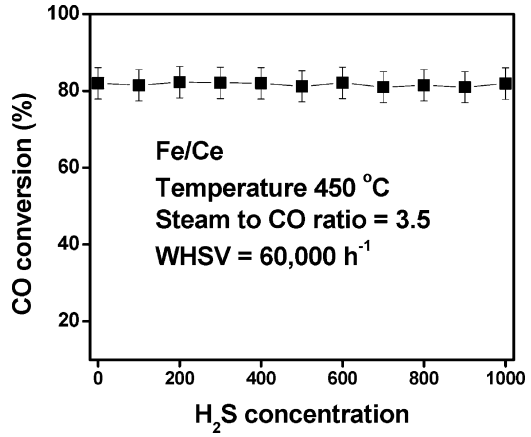

Figure 4. Effect of H_2S content on the WGS activity of Fe/Ce (temperature = 450 °C, WHSV = 60 000 h^{-1}, steam to CO ratio = 3.5).

Properties of Fresh Catalysts. BET surface area and crystallite size values of hematite in all M-modified and Cu codoped M-modified ferrite fresh catalysts are presented in Table 1. All Cu codoped catalysts exhibit higher surface area and smaller crystallite size than M-modified ferrites. The increase in the surface area is due to incorporation of Cu^{2+} ions into the hematite lattice and formation of a solid solution. All M-modified ferrites and Cu codoped M-modified ferrites exhibit nanosized grains. X-ray diffraction patterns of both M-modified and Cu codoped M-modified ferrite freshly calcined catalysts (not shown) typically exhibit reflections from the hematite phase. Interestingly, upon the addition of Cu, a distinct shift in the XRD peak position was observed which indicates that some compositional changes were also taking place. The shift is due to the incorporation of the Cu^{2+} ion into the Fe_2O_3 crystal lattice and forming solid solutions. There are no peaks corresponding to either metal or compounds between iron and the metal in M-modified ferrites except for the case of Fe/Ce. In addition to reflections from the hematite phase, a few more reflections were observed at 2θ = 30 and 56° in the case of Fe/Ce and Fe/Ce/Cu catalysts. These reflections primarily belong to the cubic ceria phase. Similarly, there are no peaks due to either CuO or compounds between Cu and iron in Cu codoped M-modified ferrites. Both Fe and Cu can form $CuFe_2O_4$ spinels very easily when mixed together. In the present study, we did not observe any formation of such spinels for our Cu codoped modified ferrites. This is due to the lower doping amount of copper (2.5%) used in this study.

Table 1. BET Surface Area and Crystallite Size Values of Various M-Modified and Copper Codoped M-Modified Ferrite Fresh Catalysts

sample	BET surface area (m^2/g)	crystallite size (nm)	composition of the catalysts by EDAX
Fe/Cr	81	15	
Fe/Cr/Cu	98	11	9.8:1.05:0.26
Fe/Ce	96	9	
Fe/Ce/Cu	126	Nd	9.75:1.0:0.23
Fe/Ni	80	12.5	
Fe/Ni/Cu	98	9.7	9.95:0.99:0.21
Fe/Co	41	8.9	
Fe/Co/Cu	80	5.8	9.9:0.95:0.25
Fe/Mn	175	18.5	
Fe/Mn/Cu	175	17.9	9.8:1:0.24
Fe/Zn	47	26	
Fe/Zn/Cu	53	22	10:1.1:0.24

Temperature-programmed reduction measurements were performed to investigate the role of Cu on reducibility of the hematite and other oxides present in the M-modified ferrites. In the reported TPR of pure hematite (Fe_2O_3), the first reduction peak appears at 302 °C, corresponding to the transition of Fe_2O_3 to Fe_3O_4. The second peak at 354 °C was attributed to the transformation of Fe_3O_4 to FeO. The third and final peak at 475 °C corresponds to the transition of FeO to Fe.[38] In another report, a peak assigned to magnetite formation showed a TPR curve at 510 °C, and another around 770 °C, attributed to the formation of metallic iron.[39] The position of the temperature maxima may vary from sample to sample depending on the particle size and other parameters such as temperature ramp rate. The addition of a substituent/dopant ion significantly modifies the reduction profile, as compared to that of the pristine Fe_2O_3 sample.[40] The TPR profiles of M-modified ferrites are reported in our earlier publication.[41] The corresponding T_{max} values of each reduction step in both M-modified and Cu codoped M-modified ferrites are shown in Table 2. In the present study, the TPR peaks were assigned on the basis of our previous results as well as literature reports.[23,39] All M-modified ferrites exhibit two types of reduction processes, namely, the reduction process of iron oxide and the reduction process of other metal oxide. The reduction process of iron oxide, i.e., $Fe_2O_3 \rightarrow Fe_3O_4 \rightarrow FeO \rightarrow Fe$, depends on the other metal oxide present in M-modified ferrites. For example, doping Cr into the iron oxide did not improve the reducibility of either hematite to magnetite or magnetite to wustite. Similarly, the reduction of temperature of $Cr^{6+} \rightarrow Cr^{3+}$ was also unaffected in the Fe/Cr catalyst when compared with pristine chromium oxide. On the other hand, promoting iron oxide with cerium causes the T_{max} of the transitions of both hematite-to-magnetite and magnetite-to-wustite to shift to lower temperatures. Also, the ceria surface shell reduction in the case of the Fe/Ce system occurs at 380

Table 2. T_{max} (°C) Values of Various Phase Transformations of the M-Modified and Copper Codoped Modified Ferrite Catalysts

sample	$Fe_2O_3 \rightarrow Fe_3O_4$	$Fe_3O_4 \rightarrow FeO$	other metal oxide reduction
Fe/Cr/Cu	350	>700	225 ($Cr^{6+} \rightarrow Cr^{3+}$)
Fe/Cr	429	>700	225
Fe/Ce/Cu	286	300	160 (ceria surface)
Fe/Ce	310	577	380
Fe/Ni/Cu	216	608	310 ($Ni^{2+} \rightarrow Ni$)
Fe/Ni	327	597	313
Fe/Co/Cu	196	598	293 ($Co_3O_4 \rightarrow CoO$)
Fe/Co	330	680	300
Fe/Mn/Cu	213	734	202 ($Mn^{4+} \rightarrow Mn^{2+}$)
Fe/Mn	300	613	200
Fe/Zn/Cu	204	713	465 ($Zn^{2+} \rightarrow Zn$)
Fe/Zn	333	700	470

dx.doi.org/10.1021/jp301090d | J. Phys. Chem. C 2012, 116, 11019−11031

°C, instead of 485 °C as in the pristine ceria sample. However, the ceria bulk reduction is not affected by the presence of iron. Similarly, the addition of Mn, Co, Ni, and Zn to the iron oxide also decreases the temperature of hematite to magnetite reduction to a small extent.

The TPR profile Cu codoped M-modified ferrites are presented in Figure 1. After codoping with Cu, all the M-modified ferrites exhibit three types of peaks, namely, the reduction process of CuO, the reduction process of Fe_2O_3, and other metal oxides. All Cu codoped M-modified ferrites exhibited CuO reduction in the temperature region 170−200 °C. Both Fe/Ce/Cu and Fe/Ni/Cu exhibit two-step reduction processes for CuO. This may be due to the presence of mass transfer limitations. An interesting reduction profile is observed for iron oxide when Cu is codoped into M-modified ferrites. Remarkably, Cu selectively promotes the reduction of hematite to magnetite but not (a) magnetite to wustite (b) wustite to metallic iron transformations in all M-modified ferrites except for the case of Fe/Ce. Interestingly, Cu also did not promote the reduction of other metal oxide presented in the M-modified ferrites except for the case of Fe/Ce. However, the codoping of Cu into the Fe/Ce catalyst promoted the reduction of (a) hematite to magnetite (b) magnetite to wustite (c) ceria surface. However, the ceria bulk reduction was unaffected. All the Cu codoped modified ferrites except Fe/Ce/Cu exhibited similar peak areas for the transitions of Fe_2O_3 to Fe_3O_4 and Fe_3O_4 to FeO. For the Fe/Ce/Cu catalysts, the peak area corresponding to the Fe_2O_3 to Fe_3O_4 transition is smaller. In the TPR profile of Fe/Ce/Cu, we observed the formation of FeO at lower temperatures. This formation of FeO is responsible for the observed lower peak area.

Properties of Activated Catalysts. *X-ray Diffraction.* To understand the unexpected behavior of Cu in M-modified ferrites, characterization measurements were performed over activated (after prereduction) catalysts. Figure 5 shows the

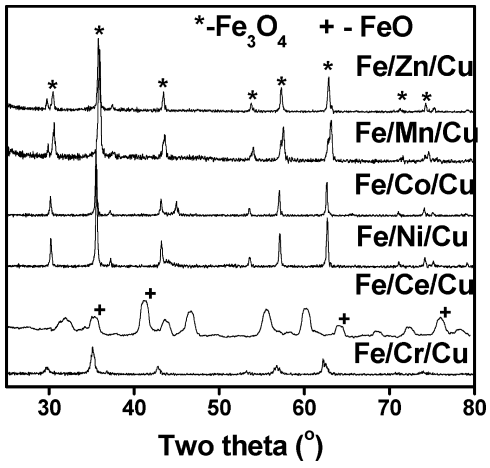

Figure 5. X-ray powder diffraction patterns of copper codoped modified ferrite activated catalysts (* - Fe_3O_4, + - CeO_2, # - FeO).

XRD diffraction patterns of the activated Cu codoped modified ferrites. As shown in Figure 5, all the catalysts display seven reflections in their XRD patterns at 17.38, 29.88, 35.58, 43.18, 53.48, 57.08, and 62.58°. These are identified with the Fe_3O_4 (magnetite) inverse cubic spinel phase. The iron oxide magnetite $Fe^{3+}(Fe^{2+}Fe^{3+})O_4$ is a classic example of an inverse spinel ferrite AB_2O_4, in which oxygen atoms approximately form a close-packed face centered cubic arrangement. The iron atoms occupy two crystallographically distinct sites, being tetrahedrally and octahedrally coordinated by oxygen anions. The inverse nature of this spinel implies that the A-sites are occupied by Fe^{3+} ions, while an equal number of Fe^{2+} and Fe^{3+} cations share the B-site. The dynamic electronic disorder (hopping) resulting from the rapid electron exchange between Fe^{2+} and Fe^{3+} cations on the B-site is responsible for the WGS activity of magnetite at high temperatures. The redox properties and activity of the various ferrite-based catalysts prepared in this study depend on the defect chemistry, and appear to be determined by critical parameters of the doped cation, such as ionic size and valence. In addition to the reflections due to the magnetite phase, the Fe/Ce/Cu catalyst exhibits a few more additional reflections at 2θ = 36, 41, and 60°. These reflections primarily belong to the wustite (FeO) phase (PDF- ICDD − 01-075-1550).[42] These results show that the simultaneous precipitation of Fe along with Ce and Cu leads to the formation of FeO during the activation. We know that FeO is an inactive phase for the WGS reaction. The formation of FeO during the activation of Fe/Ce/Cu is responsible for the lower WGS activity compared to the Fe/Ce catalyst. TPR results presented earlier also suggest that the transformation of magnetite to wustite occurs around 200 °C. In all the other ferrites, this transformation occurred above 500 °C. There are no reflections from either CuO or compounds of Cu and Fe_3O_4. Both Fe/Ce and Fe/Ce/Cu catalysts continue to exhibit reflections due to ceria in the activated samples as well. There was no evidence for the formation of Fe (metallic) or Fe_2C phases due to over-reduction in any of the M-modified or Cu codoped modified ferrites. The lattice constant values were measured from the (311) plane of the magnetite phase (Figure 6).[43] By comparing

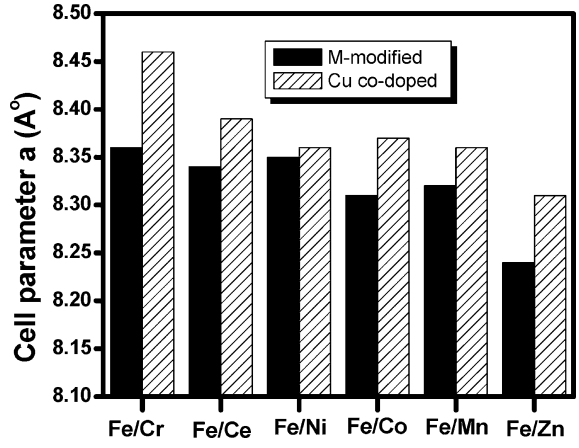

Figure 6. Cell parameter measurements plot of various M-modified and copper codoped M-modified ferrite activated catalysts.

the values of the Cu codoped modified ferrite samples with those of the M-modified ferrite samples, prepared by an identical method, we find the lattice expansion upon Cu codoping. This is due to the fact that Cu has a larger ionic radius than both Fe^{3+} and Fe^{2+}. Hence, when Cu is incorporated into the magnetite lattice, it leads to the lattice expansion.

Mössbauer Spectroscopy. Mössbauer spectroscopy has proved to be a powerful probe not only to investigate the magnetic phases but also to identify the underlying aspects of Fe local structure. The hyperfine interactions between the ^{57}Fe

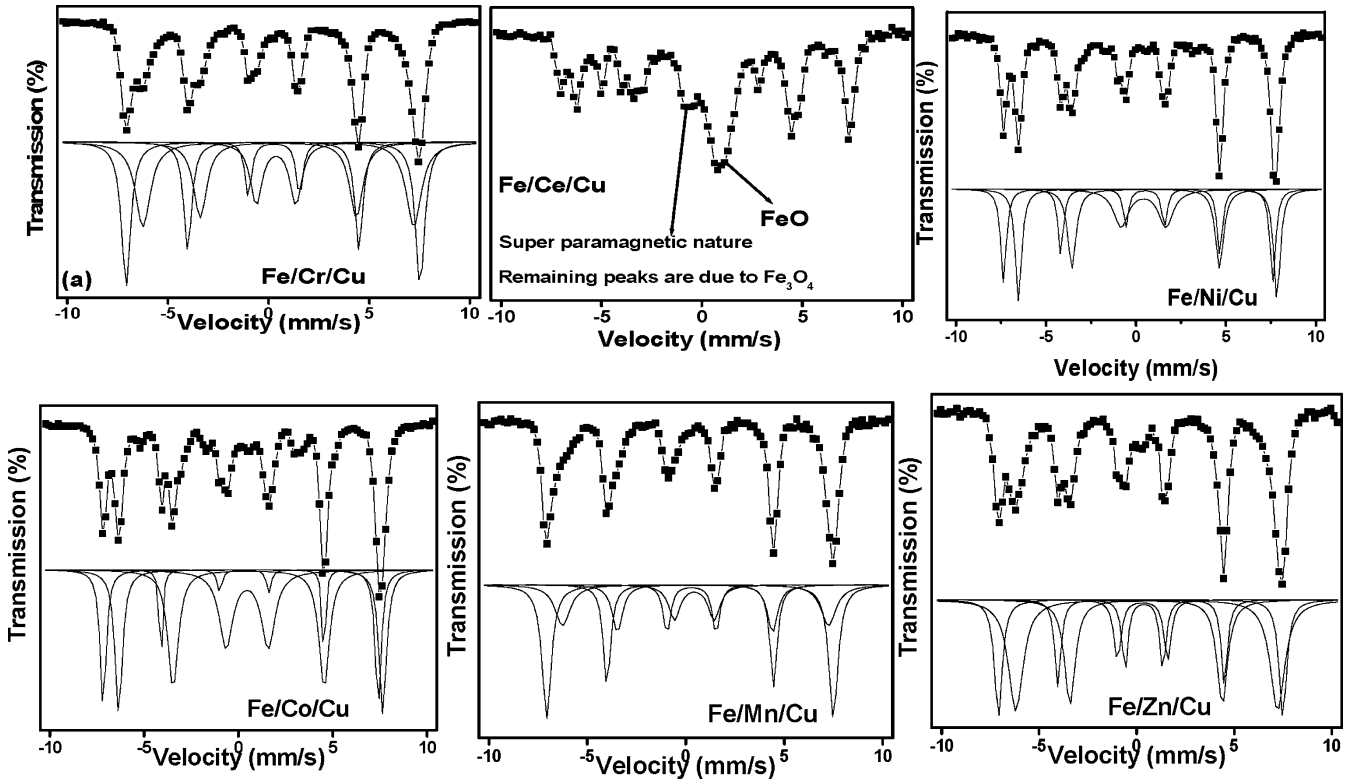

Figure 7. Mossbauer spectroscopy of activated copper codoped modified ferrites measured at room temperature.

nuclei and the electrons surrounding them are provided through the hyperfine parameters: isomer shift (δ), quadrupole splitting (Δ), and magnetic field (H). The isomer shift parameter δ is mainly related to the oxidation state of the Fe ion, Δ describes the symmetry of the charge distribution around the Fe nucleus or site distortion from cubic symmetry, and H provides information about electron spin density at the ^{57}Fe nucleus in a magnetically ordered compound. Doped magnetites seem to be an ideal illustration to identify the Fe distribution at T_d (A) and O_h (B) sites. X-ray powder diffraction measurements reveal that all the activated M-modified and Cu codoped M-modified ferrites consist of a magnetite phase. As explained earlier, magnetite has an inverse spinel structure. The unit cell consists of 32 cage O^{2-} ions in the FCC arrangement. The cations are distributed amongst the interstitial positions of the lattice. There are 64 such sites with T_d symmetry of which a maximum of 8 are occupied by Fe^{3+} ions and 32 with O_h symmetry of which a maximum of 16 are occupied by an equal number of Fe^{3+} and Fe^{2+} ions. In stoichiometric magnetite, all the interstitial sites are occupied by Fe^{3+} and Fe^{2+} ions. In nonstoichiometric or doped magnetite, some sites are either empty or occupied by guest cations. Magnetite undergoes a metal−insulator transition near 120 K (T_V), known as the Verwey transition.[44−48] It is characterized by a large decrease in conductivity and drop of the magnetization, as well as by a heat capacity anomaly below the transition temperature.[49] In addition, the crystal symmetry is lowered from cubic to monoclinic. In principle, one might expect three different Fe sites in magnetite: one from the Fe^{3+} ions at T_d sites, one from the Fe^{3+} ions at O_h sites, and another from the Fe^{2+} ions in the O_h sites. Above 120 K, due to the fast electron exchange between Fe^{3+} and Fe^{2+} at O_h sites, an averaging occurs. Hence, above 120 K, a site generally identified with Fe^{3+} ions in the T_d sites, and the other with both Fe^{3+} and Fe^{2+} ions at O_h sites, i.e., one six-line hyperfine structure is due to all T_d cations, while the other is due to O_h cations. Below 120 K, a total of five sites are needed to explain the magnetic properties satisfactorily, namely, one from Fe^{3+} in T_d sites, two from Fe^{3+} in O_h sites, and two from Fe^{2+} in O_h sites in a single crystal magnetite.[50] However, in a nanosized magnetite, averaging between Fe^{3+} ions at O_h and T_d sites takes place.[9] Hence, below 120 K, the observed structure is identified: one six-line spectrum coming from Fe^{3+} ions in both sites and the other from Fe^{2+} ions.[51] In the present study, we performed Mössbauer spectroscopy measurements both at 300 and 78 K to investigate the distribution of Cu ions in the magnetite spinels.

Mössbauer spectra of Cu codoped modified ferrites at 300 K are presented in Figure 7. All the Cu codoped and M-modified ferrites show similar Mössbauer spectra except the cases of Fe/Ce and Fe/Ce/Cu. The typical spectra exhibit two well-developed six-line magnetic hyperfine structures typical of bulk materials. The high field component is due to Fe^{3+} ions at T_d sites, while the low field one arises from Fe^{2+} and Fe^{3+} ions present at O_h sites.[52] The δ and H values presented in Table 3 are in good agreement with previous reports.[53−55] There is not much change in the δ values for Fe at T_d sites after Cu codoping. On the other hand, δ values for O_h (low field component) in the Cu codoped M-modified ferrite catalysts are noticeably higher than those in M-modified ferrite catalysts at 300 K (Table 3). The O_h/T_d fractions in Cu codoped and M-modified ferrite catalysts appear in Table 3. Generally, this ratio is close to 2 in pure activated Fe_2O_3 catalyst.[52] However, in the Cu codoped ferrite catalysts, the fraction decreases compared to the one in M-modified ferrite catalysts. These results show that the Cu guest enters at the O_h sites of magnetite during the activation of the catalysts, and alters the local structure. The Mössbauer line shapes of both Fe/Ce and Fe/Ce/Cu ferrite

dx.doi.org/10.1021/jp301090d | J. Phys. Chem. C 2012, 116, 11019−11031

Table 3. Isomer Shift (δ), Magnetic Field (H), and Concentration Ratio of Octahedral to Tetrahedral Site Values in Various M-Modified and Copper Codoped Modified Ferrite Catalysts[a]

	tetrahedral sites		octahedral sites		
sample	δ (mm/s)	H (KOe)	δ (mm/s)	H (KOe)	Oh/Td
Fe/Cr/Cu	0.32	485	0.53	447	1.1
Fe/Cr	0.32	513	0.47	475	2.54
Fe/Ce/Cu	ND	ND	ND	ND	ND
Fe/Ce	0.33	509	0.47	471	2.44
Fe/Ni/Cu	0.31	480	0.53	460	1.3
Fe/Ni	0.31	498	0.50	478	1.8
Fe/Co/Cu	0.3	485	0.58	465	1.4
Fe/Co	0.32	493	0.52	472	2.6
Fe/Mn/Cu	0.33	484	0.49	449	1.5
Fe/Mn	0.33	487	0.47	454	1.9
Fe/Zn/Cu	0.33	485	0.48	446	1.6
Fe/Zn	0.33	489	0.47	440	1.9

[a]The Mössbauer spectroscopy measurements were carried out at room temperature.

differ from other modified ferrites; in the case of Fe/Ce catalyst, in addition to the two six-line patterns, a broad singlet is observed at the near zero mm/s. This singlet is due to the super paramagnetic behavior of the catalysts, resulting from a collapse of the H-field in the nanosized particles. The Mössbauer spectrum of Fe/Ce/Cu exhibits additional peaks at a velocity of 1.5 mm/s along with the two six-line magnetic hyperfine structures. These peaks primarily belong to the wustite phase.[56] Hence, our original Mössbauer spectroscopic investigations corroborate with XRD and TPR measurements.

Figure 8 represents the Mössbauer spectra of Cu codoped modified ferrites measured at 78 K. The spectra show two well-developed six-line magnetic hyperfine structures typical of bulk materials with no trace of super-paramagnetic behavior except Fe/Ce/Cu. The lower field spectrum is due to Fe^{2+} ions at O_h sites, while the high field spectrum arises from Fe^{3+} ions at both O_h and T_d sites (Table 4). The isomer shift and magnetic field

Table 4. Isomer Shift (δ), Magnetic Field (H), and Concentration Ratio of Fe^{3+}/Fe^{2+} Ion Values in Various M-Modified and Copper Codoped Modified Ferrite Catalysts[a]

	Fe^{3+}		Fe^{2+}		
sample	δ (mm/s)	H (KOe)	δ (mm/s)	H (KOe)	Fe^{3+}/Fe^{2+}
Fe/Cr/Cu	0.33	511	0.49	474	1.9
Fe/Cr	0.33	511	0.39	446	1.4
Fe/Ce/Cu	ND	ND	ND	ND	ND
Fe/Ce	0.33	505	0.47	470	1.4
Fe/Ni/Cu	0.36	507	0.53	479	2.0
Fe/Ni	0.36	507	0.46	470	1.5
Fe/Co/Cu	0.37	508	0.46	478	2.45
Fe/Co	0.35	510	0.41	460	1.75
Fe/Mn/Cu	0.34	519	0.47	485	2.3
Fe/Mn	0.35	517	0.42	470	1.8
Fe/Zn/Cu	0.33	512	0.49	480	2.1
Fe/Zn	0.33	514	0.47	470	1.9

[a]The Mössbauer spectroscopy measurements were carried out at liquid nitrogen temperature (78 K).

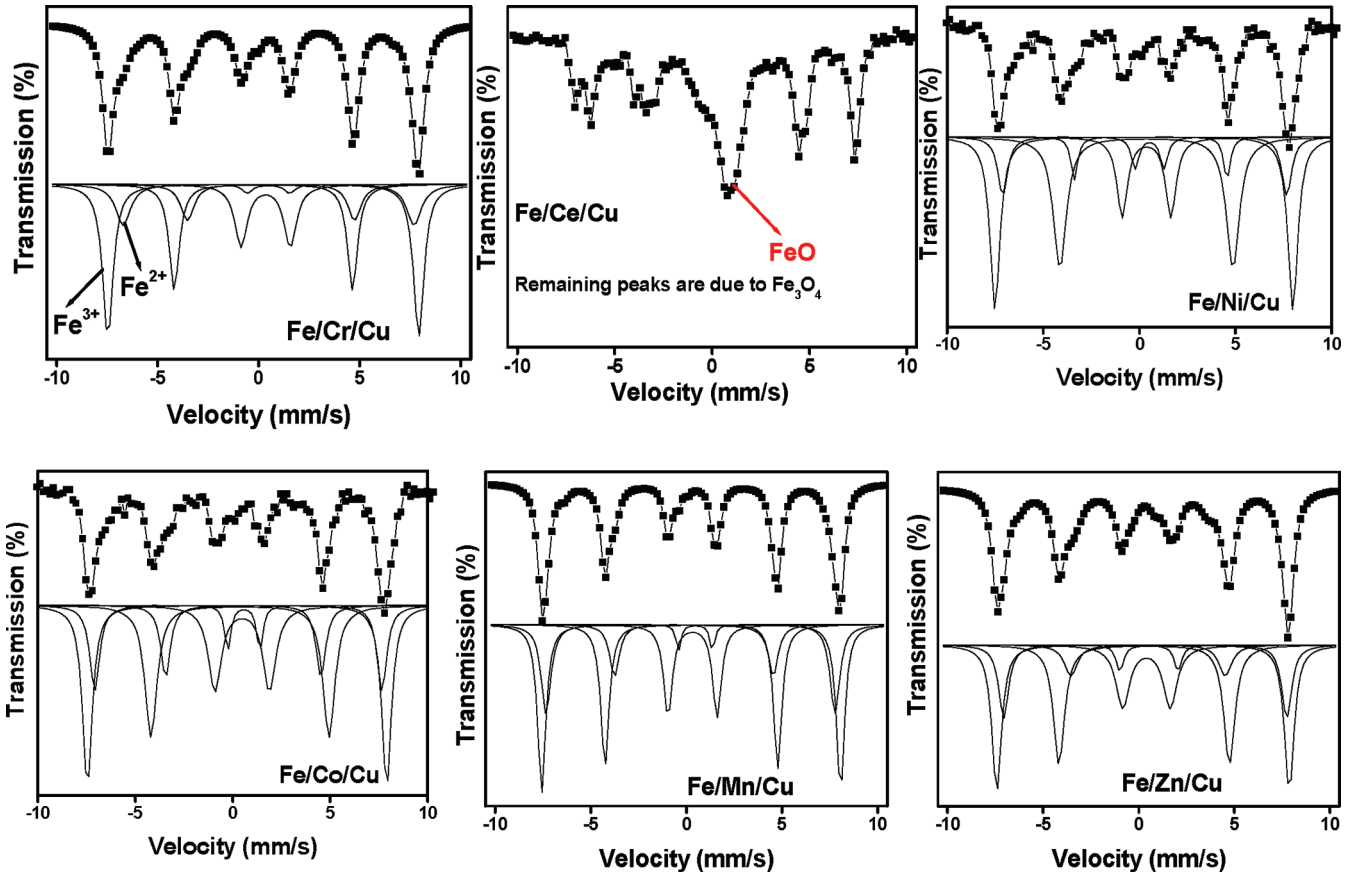

Figure 8. Mossbauer spectroscopy of activated copper codoped modified ferrites measured at liquid nitrogen (78 K) temperature.

dx.doi.org/10.1021/jp301090d | J. Phys. Chem. C 2012, 116, 11019−11031

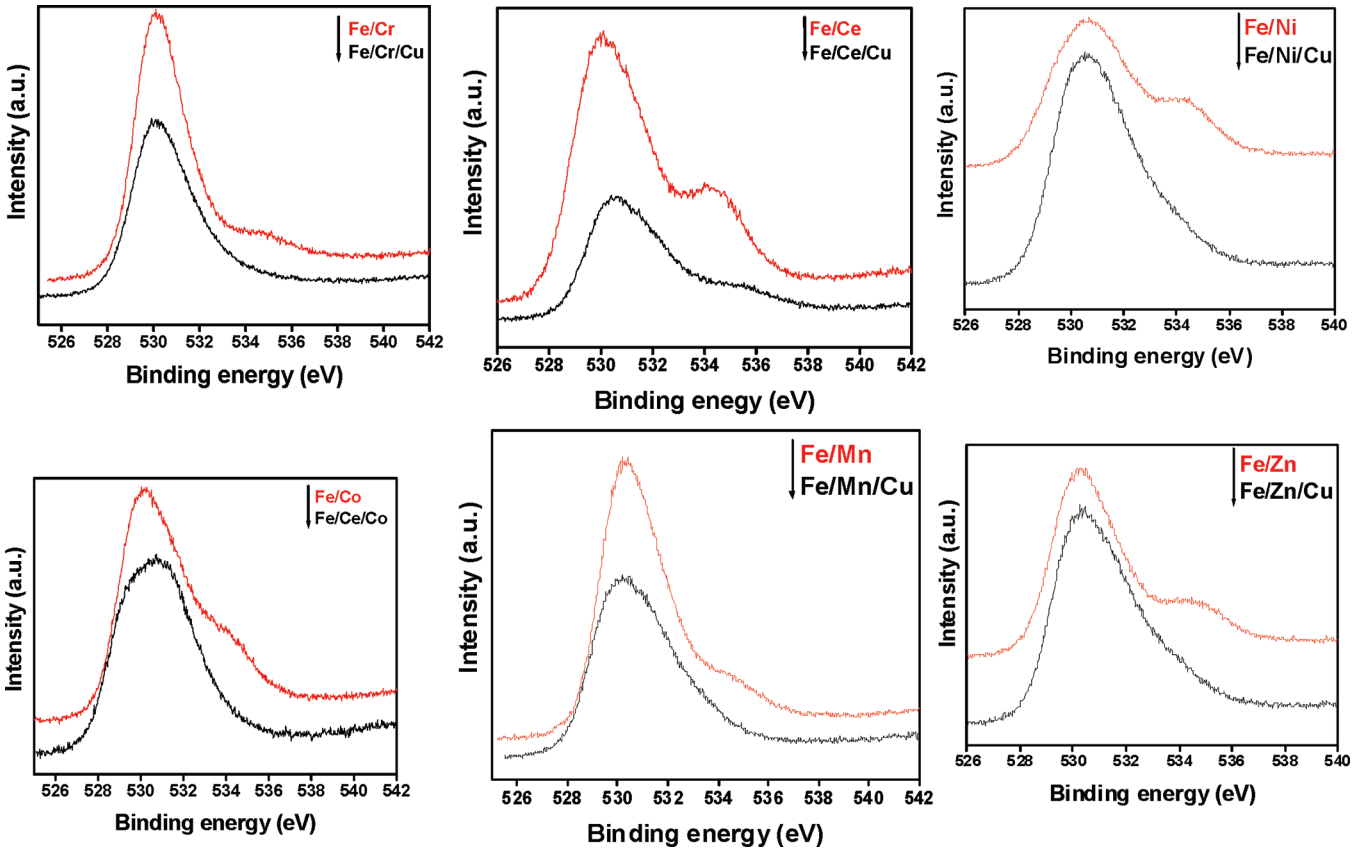

Figure 9. O1s XPS spectra of various M-modified and copper codoped modified ferrite catalysts.

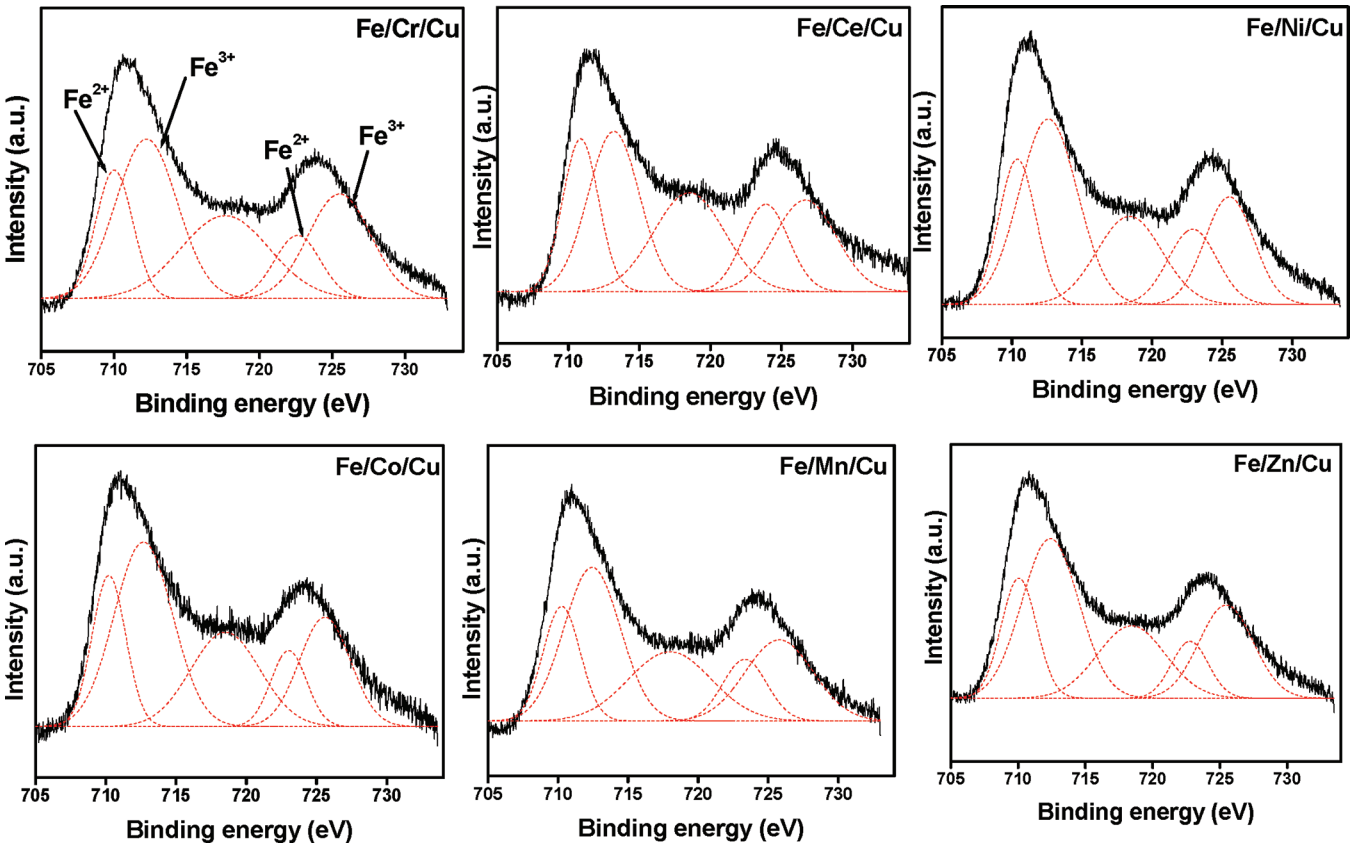

Figure 10. Fe2p XPS spectra of various copper codoped modified ferrite catalysts.

dx.doi.org/10.1021/jp301090d | J. Phys. Chem. C 2012, 116, 11019−11031

values presented in Table 4 are in good agreement with previous reports.[55] The Fe^{3+}/Fe^{2+} fractions in Cu codoped and M-modified ferrite catalysts are presented in Table 4. All Cu codoped and M-modified ferrites exhibited higher Fe^{3+}/Fe^{2+} fractions compared to the M-modified ferrites. Sorescu et al.[57] reported that with increasing Mn content the magnetite relative area of the Fe^{2+} ions decreases due to the Mn^{2+} ions substituting Fe^{2+} ions at O_h sites and the relative area of the Fe^{3+} ions increases accordingly. These results suggest that Cu replaces the Fe^{2+} ions at octahedral sites except for the case of Fe/Ce/Cu. On the other hand, formation of FeO was continued in Fe/Ce/Cu at liquid nitrogen temperature. On the whole, Mössbauer spectroscopic results show that Cu enters at octahedral sites of the magnetite during the activation and replaces the Fe^{2+} ions at the O_h sites and promotes the WGS activity except for the Fe/Ce/Cu. However, the addition of Cu to the Fe/Ce catalyst leads to the formation of the wustite phase upon the activation and decreases the WGS activity.

X-ray Photoelectron Spectroscopy. To understand the nature of interactions between iron and metal guest atoms in M-modified ferrites and Cu codoped M-modified ferrites, XPS measurements were undertaken. The photoelectron peaks of O1s and Fe 2p of the activated M-modified ferrites and Cu codoped M-modified ferrites are presented in Figures 9 and 10. The corresponding electron binding energies of O1s, Cu2p, and Fe2p photoelectron peaks are shown in Table 5. As represented in Figure 9, the O 1s spectra of M-modified ferrites and Cu codoped M-modified ferrites are broad and complicated due to overlapping contribution from iron and other metal in M-modified ferrites and Fe, Cu, and other metal in the case of Cu codoped M-modified ferrites.[58] According to literature reports, the O 1s binding energies of Fe_3O_4 and CuO are 529.7 and 530.2 eV, respectively.[59] The binding energy of the most intense peak in the case of M-modified ferrites is observed at 529.8 eV, and it mainly belongs to oxygen atoms that are bound to Fe, judging from the differences in the electronegativity of the elements involved and from the literature.[60] In addition to the peak at 529.8 eV, M-modified ferrite catalysts also exhibit a peak near 534 eV. This peak appeared due to the formation of carbonate species in the activation process. During the activation, we used process gas (mixture of CO, CO_2, H_2, and steam) to convert hematite into active magnetite. The carbonate formation occurs via reaction with either CO or CO_2. After codoping with Cu, not much changes in the O1s binding energy of M-modified ferrite catalysts, which indicates that on the surface of the these catalysts most of the oxygen species are bound to the Fe. Interestingly, the peak due to the carbonate formation is not observed in any of the Cu codoped M-modified ferrite activated catalysts. These results demonstrate that Cu codoping in the M-modified ferrites suppresses carbonate formation during the activation. To validate the carbonate formation, we also measured C 1S spectra of M-modified ferrites and Cu codoped M-modified ferrites. All M-modified ferrites exhibit a peak due to the carbonate species at 288.6 eV, and Cu codoped M-modified ferrites exhibit only a peak due to the carbon grid. We also measured O1s spectra of Fe/Ni, Fe/Mn, Fe/Ni/Cu, and Fe/Mn/Cu samples after heating the samples at 200 °C. The peak due to carbonate was observed in the case of Fe/Ni and Fe/Mn catalysts, and the carbonate peak was not observed in the corresponding Cu codoped modified ferrites. These results conclude that all the M-modified ferrites form carbonate during the activation and addition of Cu suppresses the carbonate formation.

Table 5. XPS Core Level Binding Energies of Various M-Modified and Copper Codoped Modified Ferrite Catalysts

		Fe 2p		
sample	O1s	Fe^{3+}	Fe^{2+}	Fe^{3+}/Fe^{2+} fraction
Fe/Cr/Cu	530.1	711	714	1.98
Fe/Cr	530.1	710.9	714	2.08
Fe/Ce/Cu	530.5	709.7	712.5	1.45
Fe/Ce	530	710.9	713.7	1.99
Fe/Ni/Cu	530.5	710.9	714.3	2.1
Fe/Ni	530.6	710.8	714.2	1.93
Fe/Co/Cu	530.3	710.6	713.8	1.92
Fe/Co	530.1	710.5	714	2.1
Fe/Mn/Cu	530.3	710.9	714	1.96
Fe/Mn	530.2	711	714.2	1.91
Fe/Zn/Cu	530.3	710.9	713.9	2.2
Fe/Zn	530.3	711	713.7	1.92

Figure 10 represents the Fe2p spectra of Cu codoped M-modified ferrites. The corresponding binding energy values are presented in Table 5. Both M-modified and Cu codoped M-modified ferrites exhibit similar XPS patterns. All the samples display two peaks at 710 and 724 eV which could be attributed to the ionization of $Fe2p_{3/2}$ and $Fe2p_{1/2}$ electrons, and with a spin orbit coupling (ΔE) of 13.9 eV. These parameters solely correspond to a Fe^{3+} and Fe^{2+} surface species in Fe_3O_4.[61] This is in good agreement with the XRD and Mössbauer data, which also showed the presence of a crystalline Fe_3O_4 phase in activated samples. The Fe^{3+} and Fe^{2+} species can be identified by two peaks near 712.0 and 710.0 eV and a satellite structure located at the high binding energy side. By deconvoluting the observed line shape as a superposition of Gaussian profiles, the Fe^{2+}/Fe^{3+} fraction on the surface of the magnetite phase was established.[62] The details of the curve-fitting procedure are as follows: (1) Select binding energy range for background subtraction. (2) Select the linear method for the background subtraction. (3) Select the Gaussian profile for peak line shape. (4) Select the asymmetry factor as 1. (5) Obtain integrated area for the specific peaks. (6) Obtain best fitted curve for experimentally obtained Fe2p, which minimizes chi square. These steps were repeated until the lowest chi square was obtained. The Fe^{3+}/Fe^{2+} fraction for M-modified ferrites and Cu codoped M-modified ferrites are reproduced in Table 5. The M-modified and Cu codoped M-modified ferrites display similar Fe^{3+}/Fe^{2+} ratios except for the special case of Fe/Ce/Cu. However, Fe/Ce/Cu catalyst shows a reduced Fe^{3+}/Fe^{2+} fraction (1.45) compared to the Fe/Ce catalyst (1.98). This is due to the formation of the wustite phase during the activation, as suggested by the XRD and Mössbauer measurements. To validate our Fe2p XPS results, we measured Fe3p spectra of some of the M-modified and Cu codoped modified ferrites. Although the Fe 3p peak consists of both Fe $3p_{3/2}$ and Fe $3p_{1/2}$, a single peak was observed in the XPS spectrum obtained from the present study. This separation energy of the XPS peaks is proportional to the spin−orbit coupling constant, which depends on the value of $1/r^3$ (where r is a radius) for the particular orbit; thus, the peak separation becomes smaller toward the outer shell.[63] Treating the Fe 3p peak as a single peak, the Fe^{3+}/Fe^{2+} ratio was determined for the Fe/Ni, Fe/Mn, Fe/Ni/Cu, and Fe/Mn/Cu catalysts. The Fe^{3+}/Fe^{2+}

fractions derived from Fe3p spectra agreed well with the fractions derived from the Fe2p spectra. These results suggest that Cu replaces the Fe^{2+} ions in the magnetite phase in the bulk. The $Cu2p_{3/2}$ spectrum of the activated ferrite exhibits an intense peak in the binding energy range of 932−934 eV (not shown) and a satellite peak at about 942 eV which is related to metallic Cu species.[59] The large full width at half-maximum (fwhm) value seems to be strong evidence for the presence of Cu ions in different binding states except for the Fe/Ce/Cu catalyst. On the other hand, the Fe/Ce/Cu catalyst exhibits an amorphous Cu 2p spectrum compared to the other samples, that Cu species are less exposed on the catalyst surface of the Fe/Ce/Cu sample. These results suggest that Cu completely enters into the magnetite lattice of the Fe/Ce/Cu catalyst during the activation and leads to the formation of FeO which results in a reduced catalytic activity.

How does surface atomic scale Fe^{3+}/Fe^{2+} chemistry of Cu codoped M-modified magnetite particles differ from its bulk counterpart? It is useful to compare the surface Fe^{3+}/Fe^{2+} fraction (Table 5) derived from XPS with the bulk Fe^{3+}/Fe^{2+} ratio (Table 4) derived from Mössbauer spectroscopy measured at 78 K. Mössbauer spectroscopic results show that Cu^{2+} enters at O_h sites of magnetite during the activation and replaces the Fe^{2+} ions, which leads to lesser Fe^{3+}/Fe^{2+} ratios compared to M-modified ferrites. XPS results suggest that all the M-modified and Cu codoped modified ferrites exhibit similar Fe^{3+}/Fe^{2+} fractions which are closer to 2. These results suggest that Cu plays a different role on iron oxide surface and in the bulk. That is up on activation, i.e., some of the Cu enters at the O_h sites of the magnetite and the remaining Cu form active Cu metallic assemblies on the surface of the magnetite. Hence, our results suggest that Cu codoping plays a dual promotional role in M-modified ferrites, namely, providing active metallic Cu species on the surface of the iron oxide and replacing Fe^{2+} ions from the octahedral sites in the bulk. This dual promotional role is largely responsible for the observed high-temperature WGS activity in Cu codoped samples compared with the M-modified ferrites except for the special case M═Ce.

Structure−Activity Relationship. From our studies, it is observed that precipitation of Fe^{3+} along with Cu^{2+}/M^{n+} leads to the formation of a hematitic solid solution of type $Fe_{0.875}M_{0.1}Cu_{0.025}$ with M = Cr, Ce, Ni, Co, Mn, and Zn. After activation, the catalysts are transformed into magnetite inverse or mixed spinels. The Fe/Ce/Cu catalyst exhibited the wustite phase along with the magnetite phase in the activated catalyst. Our shift activity measurements suggested that Cu acts as a promoter for all the M-modified ferrites except for Fe/Ce/Cu. However, the addition of copper to the Fe/Ce sample decreases the shift activity compared to the Fe/Ce catalyst. Among the various catalysts investigated, Fe/Ce, Fe/Cr/Cu, and Fe/Ni/Cu catalysts exhibited equilibrium conversion at the reaction temperature 550 °C. TPR measurements reveal that the addition of copper to the modified ferrites shifts the temperature maxima of hematite to magnetite to lower temperatures and promotes the WGS activity. However, Cu does not promote the reduction of magnetite to wustite or reduction of other metal oxides present in the ferrite except for the special case M═Ce. TPR results also indicate that the addition of Cu to the Fe/Ce brought the reduction temperature of the $Fe_3O_4 \rightarrow FeO$ transformation and surface ceria reduction to much lower temperatures (200 °C). XRD results revealed the formation of the wustite phase along with the magnetite during the activation of the Fe/Ce/Cu catalyst. Mössbauer spectra and cell parameter measurements show that Cu ions enter at O_h sites of the magnetite and replace Fe^{2+} ions except for Fe/Ce/Cu. XPS measurements indicate that Cu forms active metallic copper species on the surface of the iron oxide except for Fe/Ce. Comparing the Fe^{3+}/Fe^{2+} fraction derived from the Mössbauer spectra and XPS measurements shows that copper plays different roles in the bulk and the surface. On the whole codoping with Cu into M-modified ferrites enters some amount at the O_h sites of the magnetite and replaces Fe^{2+} ions and remaining Cu forms metallic Cu species on the surface of the magnetite during the activation and in general promotes the WGS activity expect for the special case M═Ce. Idakiev[20] et al. reported that Cu^{2+} cations form a solid solution with Fe^{2+} and Fe^{3+} and modify electronic properties of the Fe_3O_4 structure during WGS reduction−oxidation sequences. Rhodes[22] et al. studies show that the presence of CuO in solid solution within the chromium doped Fe_3O_4 leads to an enhancement in catalyst activity for the water−gas shift reaction. Andreev et al.[21] have proposed that the Cu promoter acts by providing new active sites similar to those present in low temperature shift catalysts comprising metallic Cu. Our characterization measurements suggest that the Cu^{2+} ion enters at the octahedral sites and forms solid solutions which leads O_h sites to contract, and an improvement in covalency of the system results and promotes electron hopping between these sites ($Fe^{2+} \leftrightarrow Fe^{3+}$), resulting in improved WGS activity. Moreover, some of the Cu form active assemblies on the surface and are responsible for the increased WGS activity in the case of Cu codoped modified ferrite catalysts except for the special case Fe/Ce. On the other hand, codoping of Cu into the Fe/Ce catalyst completely enters at the O_h sites of the magnetite and replaces Fe^{2+} ions which promote the reduction of (a) hematite to magnetite (b) magnetite to wustite (c) ceria surface. This leads to the formation of the wustite phase during the activation and inhibits the WGS activity of Fe/Ce.

4. CONCLUSIONS

The effect of the copper codoping on the structure and redox chemistry of M-modified ferrites with M = Cr, Ce, Ni, Co, Mn, and Zn has been examined using Mössbauer and XPS techniques. The high surface area $Fe_{0.875}M_{0.1}Cu_{0.025}$ type of spinels were synthesized and investigated for the high temperature WGS reaction at a steam/CO ratio of 3.5 and temperatures of 450 and 550 °C. Our shift activity results reveal that Cu acts as a promoter for all the M-modified ferrites except for the Fe/Ce. On the other hand, it acts as an inhibitor for the Fe/Ce. XRD results reveal the formation of the hematite phase in fresh catalysts and the magnetite phase in activated spinels. TPR measurements indicate that the addition of Cu to the M-modified ferrites with the exception of Fe/Ce/Cu shifts the temperature maxima of hematite to magnetite transition to lower temperatures, and promotes the WGS activity. XPS results suggest that Cu codoping into ferrites suppresses the carbonate formation upon activation. XPS results, largely a surface probe, show that Cu forms an active metallic Cu species on the surface of the magnetite except for the case of M = Ce. The Mössbauer effect results largely probing the bulk show that Cu enters at O_h sites in magnetite upon activation of the catalysts to replace Fe^{2+} ions at octahedral sites, and, in general, promotes the WGS activity except for the case of M = Ce. For the case M = Ce, (a) XRD results concluded that activation of the catalyst leads to formation of the wustite phase. (b) The

addition of Cu to the Fe/Ce catalyst decreases the transition temperature of hematite to magnetite and the transition temperature of magnetite to wustite. Cu also decreases the reduction temperature of surface ceria significantly in the Fe/Ce catalyst. (c) XPS and Mössbauer results show that Cu and Ce enter at the octahedral site of magnetite and form the wustite phase along with the magnetite phase. Because of the presence of wustite, the performance of the Fe/Ce/Cu catalyst is lower than the Fe/Ce. Hence, our characterization measurements show that copper changes the redox chemistry of the $Fe^{2+} \leftrightarrow Fe^{3+}$ couple of the magnetite during the activation, responsible for either promotion or inhibition of the WGS activity.

AUTHOR INFORMATION

Corresponding Author

*Phone: +1 513 556 1474. Fax: +1 513 556 3473. E-mail: panagiotis.smirniotis@uc.edu.

Notes

The authors declare no competing financial interest.

ACKNOWLEDGMENTS

Financial support was provided by the U.S. Department of Energy (grant DE-PS36-03GO93007). The financial support received from Ohio Air Quality Development Authority (AY08-09-C21) is also appreciated.

REFERENCES

(1) Costa, R. C. C.; Lelis, F.; Oliveira, L. C. A.; Fabris, J. D.; Ardisson, J. D.; Rios, R. R. A.; Silva, C. N.; Lago, R. M. *Catal. Commun.* **2003**, *4*, 525−529.

(2) Selim, M. S.; Turky, G.; Shouman, M. A.; El-Shobaky, G. A. *Solid State Ionics Diffusion React.* **1999**, *120*, 173−181.

(3) Ramankutty, C. G.; Sugunan, S.; Thomas, B. *J. Mol. Catal. A: Chem.* **2002**, *187*, 105−117.

(4) Oliveira, L. C. A.; Rios, R. V. A.; Mussel, W. N.; Fabris, J. D.; Lago, R. M. *Stud. Surf. Sci. Catal.* **2000**, *130*, 2165−2170.

(5) Rylander, P. N.; Zimmerschied, W. J. U.S. Patent 1957, 2,805,187.

(6) Rennard, R. J.; Kehl, W. L. *J. Catal.* **1971**, *21*, 282−293.

(7) Kikuchi, E.; Uemiya, S.; Sato, N.; Inoue, H.; Matsuda, T. *Chem. Lett.* **1989**, 489−492.

(8) Lin, Y. S. *Sep. Purif. Technol.* **2001**, *25*, 39−55.

(9) Tang, Z.; Kim, S. J.; Reddy, G. K.; Smirniotis, P.; Dong, J. *J. Membr. Sci.* **2010**, *354*, 114−122.

(10) Lin, Y. S.; Kumakiri, I.; Nair, B. N.; Alsyouri, H. *Sep. Purif. Methods* **2002**, *32*, 229−379.

(11) Dong, J.; Liu, W.; Lin, Y. S. *AIChE J.* **2000**, *46*, 1957−1966.

(12) Daly, H.; Goguet, A.; Hardacre, C.; Meunier, F. C.; Pilasombat, R.; Thompsett, D. *J. Catal.* **2010**, *273*, 257−265.

(13) Júnior, I. L.; Millet, J-.M.M.; Aouine, M.; Rangel, M. C. *Appl. Catal., A* **2005**, *283*, 91−98.

(14) Lei, Y.; Cant, N. W.; Trimm, D. L. *J. Catal.* **2006**, *239*, 227−236.

(15) Reithwisch, D. G.; Dumesic, J. A. *Appl. Catal.* **1986**, *21*, 97−109.

(16) Boreskov, G. K. *Kinet. Katal.* **1970**, *11*, 374−382.

(17) Rylander, P. N. ; Zimmerschied, W. J. U.S. Patent 1957, 2,805,187.

(18) Keizoo, I.; Toshio, T.; Maso, K.; Toshikazu, A. *Jpn. Kokai Tokkyo Koho* **1976**, *74*, 102590−102591.

(19) Pati, R. K.; Lee, I. C.; Hou, S.; Akhuemonkhan, O.; Gaskell, K. J.; Wang, Q.; Frenkel, A. I.; Ehrman, S. H. *ACS Appl. Mater. Interfaces* **2009**, *1*, 26242435.

(20) Idakiev, V.; Mihajlo, A. D.; Kanev, B.; Andreev, A. *React. Kinet. Catal. Lett.* **1987**, *33*, 119−124.

(21) Andreev, A.; Idakiev, V.; Mihajlova, D.; Shopov, D. *Appl. Catal.* **1986**, *22*, 385−387.

(22) Rhodes, C.; Hutchings, G. J. *Phys. Chem. Chem. Phys.* **2003**, *5*, 2719−2723.

(23) Khan, A.; Chen, P.; Boolchand, P.; Simrnitios, P. G. *J. Catal.* **2008**, *253*, 91−104.

(24) Reddy, B. M.; Khan, A. *Catal. Surv. Asia* **2005**, *9*, 155−171.

(25) Klug, H. P.; Alexander, L. E. *X-ray Diffraction Procedures for Polycrystalline and Amorphous Materials*, 2nd ed.; Wiley: New York, 1974.

(26) Navrotsky, A.; Kleppa, O. J. *J. Inorg. Nucl. Chem.* **1967**, *29*, 2701−2714.

(27) Krawitz, A. D. *Introduction to Diffraction in Materials Science and Engineering*; Wiley- Interscience: New York, 2001.

(28) Boolchand, P.; Pradhan, S.; Wu, Y.; Abdelgadir, M.; Huff, W.; Forell, D.; Coussement, R.; McDaniel, D. *Phys. Rev. B* **1992**, *45*, 921−930.

(29) Rhodes, C.; Hutchings, G. J.; Ward, A. M. *Catal. Today* **1995**, *23*, 43−58.

(30) Reddy, G. K.; Kim, S. J.; Dong, J.; Smirniotis, P.; Jasinski., J. *Appl. Catal., A* **2012**, *415*, 101−110.

(31) Xue, E.; O'Keeffe, M.; Ross, J. R. H. *Catal. Today* **1996**, *30*, 107−118.

(32) Lloyd, L.; Ridler, D. E.; Twigg, M. V. In *Catalyst Handbook*, 2nd ed.; Twigg, M. V., Ed.; Wolfe Publishing Ltd.: London, 1989; p 283.

(33) Twigg, M. V. *Catalyst Handbook*, 2nd ed.; Wolfe Publishing: London, 1989; p 268.

(34) Reddy, G. K.; Gunasekara, K.; Boolchand, P.; Smirniotis, P. *J. Phys. Chem. C* **2011**, *115*, 920−930.

(35) Alonso, F. J. P.; Cabrera, I. M.; Granados, M. L.; Kapteijn, F.; Fierro, J. L. G. *J. Catal.* **2006**, *239*, 340−346.

(36) Newsome, D. S. *Catal. Rev. Sci. Eng.* **1980**, *21*, 275−318.

(37) Hla, S. S.; Duffy, G. J.; Morpeth, L. D.; Cousins, A.; Roberts, D. G.; Edwards, J. H. *Catal. Commun.* **2009**, *10*, 967−970.

(38) Wimmers, O. J.; Arnoldy, P.; Moulijn, J. A. *J. Phys. Chem.* **1986**, *90*, 1331−1337.

(39) Jung, H.; Thompson, W. *J. Catal.* **1991**, *128*, 218−230.

(40) Sastri, M. V. C.; Vishwanath, R. P.; Vishwanath, B. *Int. J. Hydrogen Energy* **1982**, *7*, 951−955.

(41) Khan, A.; Smirniotis, P. *J. Mol. Catal. A: Chem.* **2008**, *280*, 43−51.

(42) Reddy, G. K.; Smirniotis, P. *Catal. Lett.* **2011**, *141*, 27−32.

(43) Rhodes, C.; Williams, B. P.; King, F.; Hutchings, G. J. *Catal. Commun.* **2002**, *3*, 381−384.

(44) Ziese, M.; Blythe, H. J. *J. Phys.: Condens. Matter* **2000**, *12*, L13−L20.

(45) Brabers, J. H. V. J.; Walz, F.; Kronmuller, H. *J. Phys.: Condens. Matter* **2000**, *12*, 5437−5452.

(46) Muxworthy, A. R. *Earth Planet. Sci. Lett.* **1999**, *169*, 51−58.

(47) Ozdemir, O. *Geophys. J. Int.* **2000**, *141*, 351−356.

(48) Muxworthy, E. M. *Geophys. J. Int.* **2000**, *140*, 101−114.

(49) Aragon, R. *Phys. Rev. B* **1992**, *46*, 5328−5333.

(50) Eckert, H. *Mossbauer spectroscopy applied to inorganic chemistry*; Long, G. J., Ed.; Springer-Verlag: New York, 1941; Vol. 2.

(51) Bauminger, R.; Cohen, S. G.; Marinov, A.; Oper, S.; Segal, K. *Phys. Rev.* **1961**, *122*, 1447−1450.

(52) Reddy, G. K.; Boolchand, P.; Dong, J.; Smirniotis, P. *J. Phys. Chem. C* **2011**, *115*, 7586−7595.

(53) Woude, F. V.; Sawatzky, G. A.; Morrish, A. H. *Phys. Rev.* **1968**, *167*, 533−535.

(54) Roca, A. G.; Marco, J. F.; Morales, M. P.; Serna, C. J. *J. Phys. Chem. C* **2007**, *111*, 18577−18584.

(55) Wang, J.; Wu, H. Y.; Yang, C. Q.; Lin, Y. L. *Mater. Charact.* **2008**, *59*, 1716−1720.

(56) Greenwood, N. N.; Gibb, T. C. *Mossbauer Spectroscopy*; Chapan and Hall Ltd.: London, 1971.

(57) Sorescu, M.; Dia Mandescu, L.; Brand, R. A.; Mihaila, T. *Mater. Lett.* **2004**, *58*, 885−888.

(58) Sawatzky, G. A.; Post, D. *Phys. Rev. B* **1979**, *20*, 1546−1555.

(59) Wagner, C. D.; Riggs, W. M.; Davis, L. E.; Moulder, J. F. In *Handbook of X-ray Photoelectron Spectroscopy*; Muilenberg, G. E., Ed.; Perkin-Elmer Corp.: City, MN, 1978.
(60) Imamura, I.; Ishida, S.; Taramoto, H.; Saito, Y. *J. Chem. Soc., Faraday Trans.* **1993**, *89*, 757−762.
(61) Pereira, A. L. C.; Berrocal, G. J. P.; Marchetti, S. G.; Alexilda, A. A.; de Souza, O.; Rangel, M. C. *J. Mol. Catal. A: Chem.* **2008**, *281*, 66−72.
(62) Reddy, G. K.; Boolchand, P.; Smirniotis, P. *J. Catal.* **2011**, *282*, 258−269.
(63) Yamashita, T.; Hayes, P. *Appl. Surf. Sci.* **2008**, *254*, 2441−2449.